Nanotechnology **18** (2007) 115707 (8pp) doi:10.1088/0957-4484/18/11/115707

Characterizing the elasticity of hollow metal nanowires

Changjiang Ji and Harold S Park

Department of Civil and Environmental Engineering, Vanderbilt University, Nashville, TN 37235, USA

E-mail: harold.park@vanderbilt.edu

Received 30 November 2006, in final form 9 January 2007
Published 7 February 2007
Online at stacks.iop.org/Nano/18/115707

Abstract

We have performed atomistic simulations on solid and hollow copper nanowires to quantify the elastic properties of hollow nanowires (nanoboxes). We analyse variations in the modulus, yield stress and strain for ⟨100⟩ and ⟨110⟩ nanoboxes by varying the amount of bulk material that is removed to create the nanoboxes. We find that, while ⟨100⟩ nanoboxes show no improvement in elastic properties as compared to solid ⟨100⟩ nanowires, ⟨110⟩ nanoboxes can show enhanced elastic properties as compared to solid ⟨110⟩ nanowires. The simulations reveal that the elastic properties of the nanoboxes are strongly dependent on the relative strength of the bulk material that has been removed, as well as the total surface area of the nanoboxes, and indicate the potential of ultralight, high-strength nanomaterials such as nanoboxes.

(Some figures in this article are in colour only in the electronic version)

1. Introduction

Metallic and semiconducting nanowires are being studied intensely due to their potential as the basic building blocks of future nanotechnologies. The interest in such low-dimensional nanomaterials is largely driven by the often superior physical properties that they show with respect to the corresponding bulk material. In general, the relatively large ratio of surface area to volume contributes strongly to surface and quantum confinement effects on the unique optical [1–3], thermal [4], electrical [5] and mechanical [6–8] properties of nanowires.

The majority of research on mechanical properties that has been performed on nanowires has concentrated on analysing the elastic and inelastic deformation and properties of solid wires with regular geometries, i.e. ⟨100⟩ wires with square cross sections. These efforts have resulted in a large collection of information quantifying nanowire mechanical properties for various loading conditions [9–29]; highlights include size-dependent elasticity [23, 24], phase transformations, shape memory and pseudoelastic behaviour [25–28], orientation-dependent deformation [19, 21, 22], amorphization at large strain rates [9, 11, 29] and many others.

However, as the ability to control the synthesis of nanostructures has increased in recent years, researchers have found that nanowires typically form in geometries that deviate from those previously studied [2]. In particular, many researchers have found that non-square cross section wires may be energetically favourable [30–38]; others have utilized novel techniques to synthesize hollow nanowires or nanoboxes [31, 39, 40].

While the ability to synthesize nanostructures of varying size and shape is itself important and interesting, these nanostructures of novel geometry have attracted much interest as researchers have discovered that their geometry can be utilized to engineer unique behaviour and properties. For example, geometry is known to have a large effect on the optical properties of metal nanoparticles [41]. More recent work has analysed the optical properties of hollow metallic nanostructures [31, 42]; it was found that the optical properties can be altered by hollowing out the nanostructure. From a perspective of mechanical behaviour [43], recent atomistic simulations have indicated that both surface orientation [22] and the geometry of nanowires [44] can have a first-order effect on the mechanical behaviour of FCC metal nanowires. Furthermore, ⟨110⟩ nanowires with non-square cross sections similar to those synthesized experimentally were found to have distinct deformation modes and mechanical properties as compared to square cross section wires [45].

In this work, we utilize atomistic calculations to study the elastic properties of hollow metal nanowires, which we

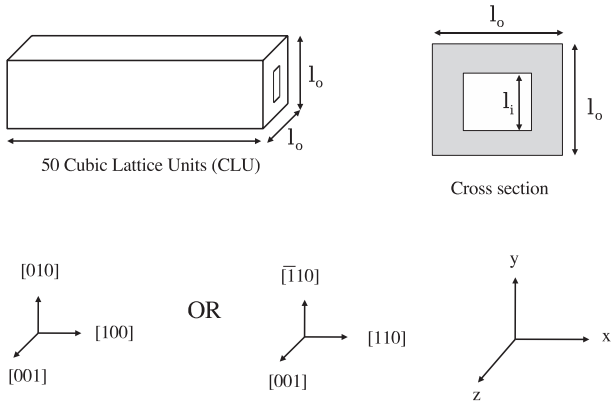

Figure 1. Schematic of the dimensions and axial orientations of the nanoboxes. Solid nanowires with square cross-sectional length l_o and same axial orientation were also considered for comparative purposes.

call nanoboxes. In doing so, we find that, while ⟨100⟩ nanoboxes are weaker than the corresponding ⟨100⟩ solid wires, ⟨110⟩ nanoboxes, which is the orientation that is most frequently observed experimentally [42], are stronger than the corresponding solid ⟨110⟩ wires. We also characterize yield stresses and strains for the nanoboxes and compare those to the values of the corresponding solid wires. These results are consistent with previous studies on solid nanowires [23, 24] that indicate that the bulk material can be either weaker or stronger, depending on the orientation. In particular, the present results indicate that geometric considerations may lead to the development of lightweight nanomaterials that offer, in certain respects, superior elastic properties that may be beneficial for future nanoengineering applications.

2. Simulation details

In this work, we performed molecular statics simulations on copper nanowires using the embedded atom method (EAM) [46, 47] as the underlying interatomic interaction model. In the EAM, the total energy U for a system of atoms is written as

$$U = \sum_{i}^{N} \left(F_i(\bar{\rho}_i) + \tfrac{1}{2} \sum_{j \neq i}^{N} \phi_{ij}(R_{ij}) \right), \qquad (1)$$

where the summations in (1) extend over the total number of atoms N in the system, F_i is the embedding function, $\bar{\rho}_i$ is the electron density at atom i, ϕ_{ij} is a pair interaction function and R_{ij} is the distance between atoms i and j. In this work, we modelled copper nanowires with the EAM potential developed by Mishin *et al* [48], which accurately represents the elastic properties and surface energies of copper.

The nanoboxes were created through a top-down approach by extracting them from a bulk copper FCC crystal. First, a solid wire was extracted, followed by removing atoms (the *bulk*) from the centre of the wire leaving a square hole and thus a hollow nanobox. As illustrated in figure 1, all nanowires and nanoboxes had the same length of 50 cubic lattice units (CLU), where 1 CLU = 0.3615 nm for copper, while both ⟨100⟩ and ⟨110⟩ longitudinal orientations were considered. The nanobox

Table 1. Cross-sectional dimensions in terms of $l_o \times l_i$ for ⟨100⟩ copper nanoboxes of length 50 CLU. All dimensions are in CLU, where 1 CLU = 0.3615 nm for copper. Equivalent solid wires of square cross-sectional length l_o were also considered for comparative purposes.

	1	2	3	4	5
Constant $(l_o - l_i)/2$	12×2	14×4	18×8	20×10	25×15
Constant l_o	20×2	20×5	20×8	20×10	20×13
Constant l_i	14×5	16×5	20×5	22×5	24×5

Table 2. Cross-sectional dimensions in terms of $l_o \times l_i$ for ⟨110⟩ copper nanoboxes of length 50 CLU. All dimensions are in CLU, where 1 CLU = 0.3615 nm for copper. Equivalent solid wires of square cross-sectional length l_o were also considered for comparative purposes.

	1	2	3	4	5
Constant $(l_o - l_i)/2$	13×3	15×5	17×7	19×9	21×11
Constant l_o	17×3	17×5	17×7	17×9	17×10
Constant l_i	13×5	15×5	17×5	19×5	21×5

cross section can be characterized with two parameters, the outer edge length l_o and the inner edge length l_i, as shown in figure 1, while the nanobox wall thickness can be defined as $(l_o - l_i)/2$. The ⟨100⟩ nanoboxes contained only {100} transverse surfaces, while the ⟨110⟩ nanoboxes contained both {100} and {110} transverse surfaces.

Solid ⟨100⟩ and ⟨110⟩ nanowires with the same length of 50 CLU square cross sections of length l_o were also studied for comparative purposes; by studying both nanoboxes and solid nanowires, we will quantify the effects of removing the bulk material on the nanobox elastic properties. Dimensions of the ⟨100⟩ solid wires and nanoboxes are given in table 1, while the ⟨110⟩ solid wires and nanobox geometries are summarized in table 2. The nanoboxes are grouped into three categories: constant wall thickness ($(l_o - l_i)/2$), constant outer edge length (l_o) and constant inner edge length (l_i).

The nanoboxes and solid wires were first relaxed to energy minimizing positions; due to the presence of tensile surface stresses [49], the nanowires and nanoboxes as extracted from the bulk are not in equilibrium, and thus contract in the longitudinal direction. After the energy minimization, the wires and boxes were quasistatically loaded in tension by fixing one end and elongating the other end using a strain increment of 0.1% while allowing relaxation of the atomic positions in the nanowire interior. The reported Young's modulus in each case was calculated by taking the slope of the stress–strain curve within the small strain regime, $\epsilon <= 0.3\%$.

In this work, we will focus on characterizing the elastic properties of the nanoboxes using three parameters: the Young's modulus, yield stress and yield strain. The modulus is generally defined as the slope of the stress/strain curve for a material under uniaxial tension, and is perhaps the most valuable elastic property as it measures the resistance, or stiffness, of the material to imposed deformation. The yield values are important as they measure how much elastic deformation, in terms of elongation (yield strain), and applied deformation (yield stress) a material can sustain before undergoing irreversible plastic deformation, or yield.

We utilize engineering strain as the strain measure in this work, while the stresses were calculated using the virial

Table 3. Normalized surface area (first value) and volume (second value) of ⟨100⟩ nanoboxes in table 1.

	1	2	3	4	5
Constant $(l_o - l_i)/2$	1.00/1.00	1.29/1.29	1.86/1.86	2.14/2.14	2.86/2.86
Constant l_o	1.00/1.00	1.11/0.95	1.21/0.85	1.27/0.76	1.36/0.58
Constant l_i	0.60/0.31	0.68/0.42	0.83/0.68	0.92/0.83	1.00/1.00

Table 4. Normalized surface area (first value) and volume (second value) of ⟨110⟩ nanoboxes in table 2.

	1	2	3	4	5
Constant $(l_o - l_i)/2$	1.00/1.00	1.25/1.25	1.50/1.50	1.75/1.75	2.00/2.00
Constant l_o	1.00/1.00	1.08/0.94	1.16/0.86	1.23/0.74	1.27/0.68
Constant l_i	0.64/0.35	0.73/0.48	0.82/0.63	0.91/0.81	1.00/1.00

theorem [50, 51], which takes the form

$$\sigma_{ij} = \frac{1}{V}\left(\frac{1}{2}\sum_{\alpha=1}^{N}\sum_{\beta\neq\alpha}^{N} U'(r^{\alpha\beta})\frac{\Delta x_i^{\alpha\beta}\Delta x_j^{\alpha\beta}}{r^{\alpha\beta}}\right) \qquad (2)$$

where N is the total number of atoms, $r^{\alpha\beta}$ is the distance between two atoms α and β, $\Delta x_j^{\alpha\beta} = x_j^{\alpha} - x_j^{\beta}$, U is the potential energy function, $r^{\alpha\beta} = \|\Delta x_j^{\alpha\beta}\|$ and V is the current volume. The yield strain and yield stress were both found at the point of initial yield, or when the first defect, which typically appears in the form of a partial dislocation, nucleates within the nanobox or nanowire.

For a nanobox, the volume was approximated as the initial volume of the solid wire minus the volume of the removed interior; this approximation is viewed as acceptable due to the fact that the modulus values we report are small strain values, and also because the nanobox geometry is largely undistorted before yield. Due to the quasistatic nature of the simulations, there are no dynamic terms that are dependent on atomic velocities in (2).

3. Simulation results

In this section, we present simulation results obtained through the tensile loading of ⟨100⟩ and ⟨110⟩ copper nanoboxes, while comparing the results obtained from the tensile loading of the corresponding solid wires of cross-sectional length l_o. Because the variations in the Young's modulus of solid nanowires have been reported in other publications [23, 24, 52], we will focus on characterizing the Young's modulus of the nanoboxes, while normalizing the modulus by that of the corresponding solid wires. Variations in yield stress and yield strain of the nanoboxes will also be considered, with comparisons made with the properties of the corresponding solid nanowires.

As various nanobox geometries have been considered in this work, we present the nanobox modulus, yield stress and yield strain in terms of the VR/TV ratio, where VR is the volume of (bulk) atoms removed to create the nanobox, and TV is the volume of the corresponding solid nanowire with cross-sectional length l_o. This ratio was calculated for nanoboxes with constant outer edge length (l_o), inner edge length (l_i) and constant nanobox wall thickness ($(l_o - l_i)/2$), and is utilized as it allows us to quantify the effects of removing increasing amounts of bulk material on the nanobox elastic properties.

For nanoboxes with a constant wall thickness, an increasing VR/TV ratio indicates an identical increase in both l_o and l_i, though the surface area to volume ratio does not change. For nanoboxes with constant outer edge length l_o, an increase in the VR/TV ratio implies a decreasing wall thickness brought on by an increase of the inner edge length l_i, while an increasing VR/TV ratio for nanoboxes with constant inner edge length l_i corresponds to a decrease in wall thickness and outer edge length l_o. To enable future discussions on the effects of surface area and volume on the elastic properties of the nanoboxes, we present normalized values for surface area and volume for the nanoboxes considered in tables 3 and 4.

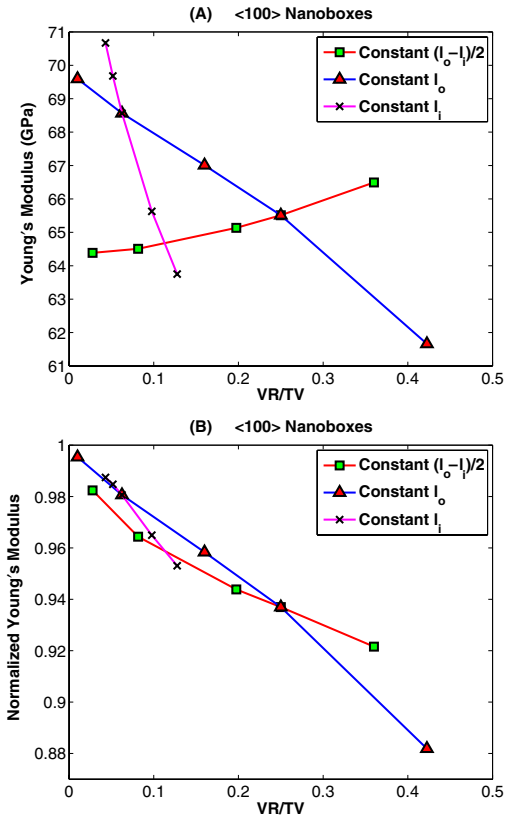

Figure 2. Variation in (A) Young's modulus and (B) normalized Young's modulus for ⟨100⟩ nanoboxes with VR/TV.

3.1. Modulus of ⟨100⟩ *nanoboxes*

Figure 2 illustrates both the actual and normalized modulus values for the ⟨100⟩ nanoboxes, which are plotted against the

VR/TV ratio. Here, the values in figure 2(B) are normalized by the computed moduli of the corresponding solid nanowires of cross-sectional length l_o.

Figure 2(A) shows variations in the measured nanobox moduli as dependent on the variations in the three different geometries considered in this work. For constant l_o and l_i nanoboxes, the modulus decreases as more of the bulk material is removed. The decrease in strength is most dramatic for the case in which the inner length l_i is kept constant, while the outer length l_o is increased. Indeed, figure 2(A) indicates that the strongest effect on the modulus comes from altering the nanobox wall thicknesses through l_o or l_i. This effect occurs due to rapid changes in surface area to volume ratio for the constant l_o and l_i nanoboxes with varying VR/TV ratio, resulting in a varying contribution to the nanobox modulus from both the bulk and surface elastic stiffnesses.

Figure 2(B) also shows variations in the nanobox modulus when normalized by the modulus for the corresponding solid wires with square cross section of length l_o. When comparing normalized values, it is clear from figure 2(B) that the ⟨100⟩ nanoboxes are elastically softer than the corresponding solid ⟨100⟩ nanowires for all nanobox geometries; furthermore, it is evident that, as more bulk material is removed in creating ⟨100⟩ nanoboxes with increasing VR/TV ratio, all nanoboxes show a corresponding decrease in modulus.

These results make a great deal of sense when analysed in the context of recent results on the relative elastic strength of bulk versus surfaces [23, 24]. In those works, it was found that, as solid ⟨100⟩ wires were gradually made smaller and smaller, their elastic modulus decreased due to the fact that the ⟨100⟩ bulk is stiffer than the {100} surfaces. The softening of the elastic properties as more bulk is removed thus matches those predictions [23, 24] and indicates that ⟨100⟩ nanoboxes will offer no stiffness enhancements as compared to the corresponding ⟨100⟩ solid wires.

Interestingly, the nanobox modulus increases slightly as seen in figure 2(A) if its wall thickness ($(l_o - l_i)/2$) is kept constant but its overall cross-sectional length including both l_i and l_o, increases; this is unexpected as this implies that more bulk material is being removed to create the nanoboxes, which would, for the ⟨100⟩ orientation, imply a decrease in modulus. Figure 2(B) thus shows that, while the modulus of the constant wall thickness nanoboxes increases slightly with increasing cross-sectional length, the rate of stiffness increase is still lower than that of the corresponding solid wires. While similar behaviour is observed and understandable for the modulus of constant thickness ⟨110⟩ nanoboxes as discussed later, it is currently unclear as to why the modulus of the constant thickness ⟨100⟩ nanoboxes increases with VR/TV.

3.2. *Yield stress and strain of* ⟨100⟩ *nanoboxes*

The yield stresses and yield strains for the various ⟨100⟩ nanoboxes are plotted in figure 3. As can be seen, for the nanoboxes with constant outer edge length l_o, both the yield stress and yield strain show a decreasing trend with increasing VR/TV ratio. The reason this occurs is because the increasing VR/TV ratio corresponds to decreasing the wall thickness by gradually increasing the inner edge length l_i. Decreasing the wall thickness corresponds to effectively removing more bulk material to create the nanoboxes; because the ⟨100⟩ bulk is stronger than the {100} surfaces, this as observed in figure 2(A) leads to a reduction in modulus.

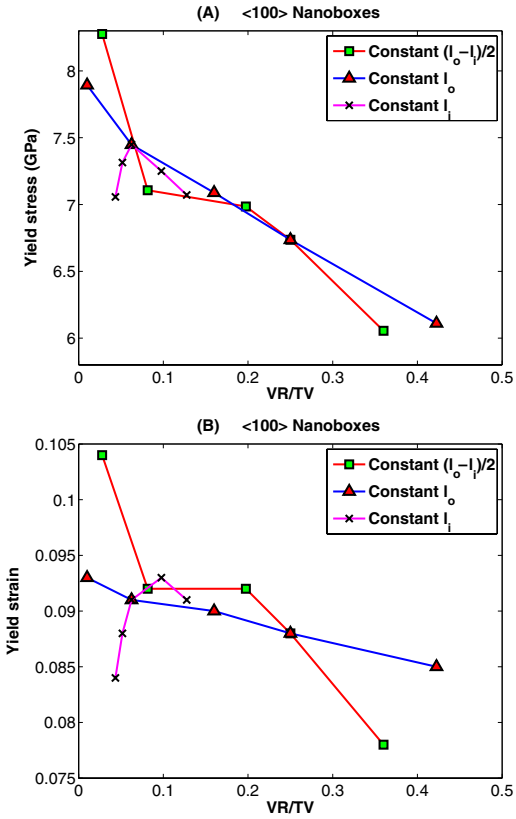

Figure 3. Variation of the (A) yield stress and (B) yield strain for ⟨100⟩ nanoboxes with VR/TV.

The yield strain decreases as VR/TV increases for the constant l_o nanoboxes because this leads to an increase in the overall surface area of the nanoboxes, as seen in table 3. This factor is critical because defects in surface-dominant nanomaterials such as nanowires tend to nucleate exclusively from surfaces, due to the fact that surfaces exist at an energetic equilibrium that is larger than that of the underlying bulk [14, 19]. Thus, the greater availability of surface area increases the likelihood of defect nucleation and initial yield, leading to reductions in yield strain and also yield stress (due to the decrease in modulus as discussed above) with increasing VR/TV for the constant l_o nanoboxes.

Similar logic can be utilized to explain the yield behaviour of the constant thickness nanoboxes. The increasing VR/TV ratio occurs due to the increase of both l_i and l_o; this increase leads to an increase of total surface area, thus resulting in the decrease in yield strain seen in figure 3(B). Although the Young's modulus increases slightly over the same range of VR/TV, the faster decrease in yield strain leads to an overall decrease in yield stress, as observed in figure 3(A).

The constant l_i nanoboxes show a slightly different response, which we now discuss. In analysing the yield strain for the constant l_i nanoboxes, it is observed in figure 3 that it shows an inconsistent trend with decreasing VR/TV ratio. In particular, with decreasing VR/TV ratio, the nanoboxes show a general decrease in yield strain; this makes sense as

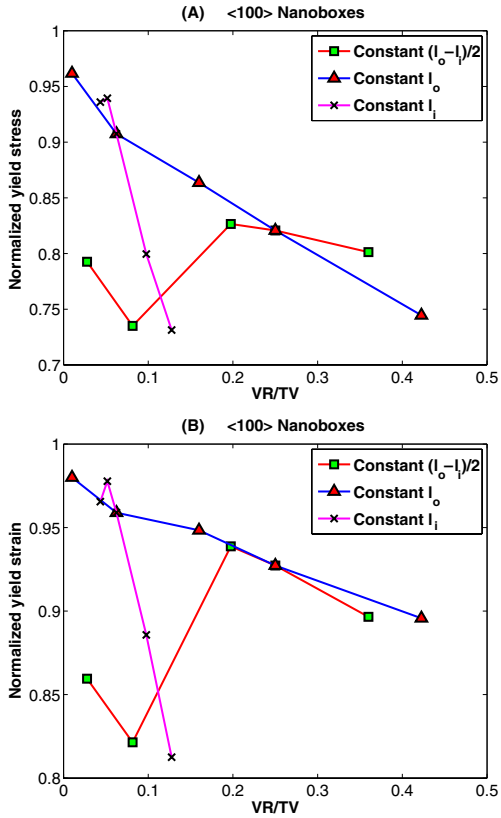

Figure 4. Variation in (A) normalized yield stress and (B) normalized yield strain of ⟨100⟩ nanoboxes with VR/TV ratio.

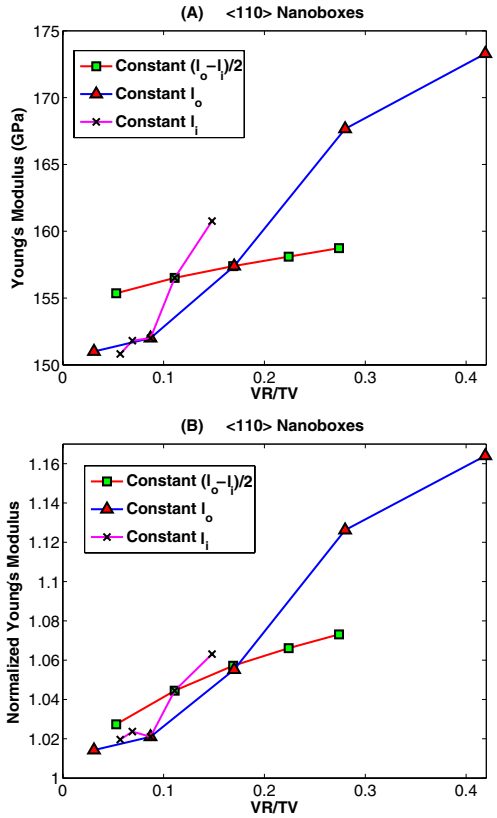

Figure 5. Variation of (A) Young's modulus and (B) normalized Young's modulus for ⟨110⟩ nanoboxes with VR/TV.

the nanobox wall thickness, and thus the surface area, increases with decreasing VR/TV, leading to enhanced opportunities for initial defect nucleation and thus reduced yield strains.

Interestingly, the constant l_i nanoboxes with the smallest wall thicknesses and thus the largest VR/TV ratios exhibited disparate yield properties, which is consistent with previous research [44] indicating that nanoboxes with ultrasmall wall thicknesses or l_i less than about 1 nm exhibit different inelastic yield behaviour. However, for larger wall thicknesses, the nanoboxes behave more like solid nanowires and the yield strain decreases as the surface area increases due to increasing l_o.

The yield stress for the constant l_i nanoboxes also shows an inconsistent trend; note that from figure 2(A), the modulus for the constant l_i nanoboxes increases with decreasing VR/TV ratio. However, because of the rapid increase in surface area with decreasing VR/TV, and thus the rapid decrease in yield strain, the increase in modulus is offset and the yield stress for the constant l_i nanoboxes begins to decrease in figure 3(A) with decreasing VR/TV.

In general, we find that not only the modulus of the ⟨100⟩ nanoboxes, but also the yield stresses and yield strains, as observed in figure 4, are reduced as compared to the corresponding solid ⟨100⟩ solid nanowires. The reduced yield strains result due to the increase in available surface area afforded to the nanoboxes; this fact, when combined with the decrease in modulus that the nanoboxes experience, explains the corresponding reductions in yield stresses for the ⟨100⟩ nanoboxes as compared to the solid ⟨100⟩ nanowires.

3.3. Modulus of ⟨110⟩ *nanoboxes*

The variations in modulus of the ⟨110⟩ nanoboxes for constant l_o, l_i and wall thickness are summarized in figure 5(A). As is illustrated, the modulus in all cases increases with increasing VR/TV ratio. The increase is largest for the nanoboxes with either constant l_o or l_i, while the modulus for the constant wall thickness nanoboxes increased only slightly.

The results are more dramatic when the moduli of the ⟨110⟩ nanoboxes are normalized by those of the corresponding ⟨110⟩ solid wires with cross sections of length l_o, as shown in figure 5(B). As can be seen, the modulus increases in all cases compared to the corresponding solid wires with increasing VR/TV ratio. For the relatively small nanobox sizes we have considered in this work, modulus increases approaching 20% are observed as compared to the corresponding solid ⟨110⟩ wires. Furthermore, the increases are attainable for all the geometries considered, while figure 5(B) indicates that even greater strength increases with respect to the solid ⟨110⟩ wires may be achievable for nanoboxes that are considerably larger than those considered in this work due to computational limitations.

The fundamental idea underlying the notion that nanostructures can be strengthened through mass removal works because it is known that the ⟨110⟩ bulk is weaker than both the {100} and {110} surfaces [23, 24] that surround the ⟨110⟩ nanoboxes and nanowires considered in this work. Therefore, because increasing the VR/TV ratio represents, in all cases, nanoboxes that are composed of decreasing amounts

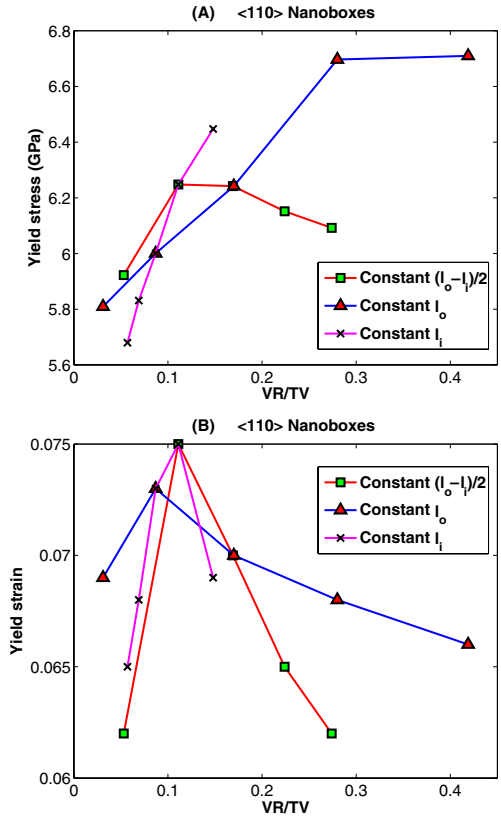

Figure 6. Variation of (A) yield stress and (B) yield strain for ⟨110⟩ nanoboxes with VR/TV.

of bulk material, all cases show corresponding increases in modulus. In this context, it is understandable why the constant thickness ⟨110⟩ nanoboxes show a slight increase in modulus with increasing VR/TV ratio as seen in figure 5, because an increase of VR/TV corresponds to the removal of more bulk material, leading to a greater dependence on the surface for strength, and thus a strength increase.

3.4. Yield stress and strain of ⟨110⟩ *nanoboxes*

The yield stresses and strains for the ⟨110⟩ nanoboxes are presented in figure 6. As can be seen, the observed trends for the yield stresses differ somewhat from those already discussed for the ⟨100⟩ nanoboxes, while the ⟨110⟩ nanobox yield strains show similar behaviour to those of the ⟨100⟩ nanoboxes.

Unlike the ⟨100⟩ nanoboxes with constant l_o, the ⟨110⟩ nanoboxes with constant l_o show a distinct increase in yield stresses with increasing VR/TV, while the yield strain decreases; the yield strain decrease is tied to the increase in surface area with increasing VR/TV. It would also be expected that the yield stress for the constant l_o nanoboxes would similarly decrease; however, due to the sharp increase in modulus with increasing VR/TV as seen in figure 5(A) with increasing VR/TV, the yield stress increases with increasing VR/TV.

For ⟨110⟩ nanoboxes with constant l_i, the trend mirrors that seen for the constant l_o ⟨110⟩ nanoboxes. For constant l_i nanoboxes, an increase in VR/TV indicates decreasing nanobox wall thickness. Correspondingly, figure 6(A) illustrates that the yield stress for the constant l_i ⟨110⟩ nanoboxes increases rapidly as l_o is reduced. Similarly, increasing VR/TV for the constant l_i nanoboxes leads to reduced wall thicknesses and thus reduced surface area, leading to an increase in the yield strain, as seen in figure 6(B).

Interestingly, the yield stress for constant l_i nanoboxes increases more rapidly with VR/TV than does the yield stress for constant l_o nanoboxes. The reason for this can be inferred from table 4, which illustrates that the volume decreases much more rapidly over the same VR/TV ratio for the constant l_i nanoboxes than for the constant l_o nanoboxes; this manifests itself in the faster increase in the modulus as seen in figure 5(A). More importantly, the surface area for constant l_i nanoboxes decreases with increasing VR/TV ratio, leading to the increase in yield strain observed in figure 6(B). Thus, the increase in modulus and yield strain with VR/TV leads the constant l_i nanoboxes to exhibit a rapid increase in yield stress.

Similar to the constant l_i ⟨100⟩ nanoboxes, the ⟨110⟩ nanoboxes with the smallest wall thicknesses or l_i (constant l_o with VR/TV $= 0.031$, constant l_i with VR/TV $= 0.148$, constant thickness with VR/TV $= 0.053$) also show unusual yield properties [44]. The small wall thicknesses of approximately 1 nm or the small l_i cause the anomalies in the yield strain trends seen in figure 6(B). As the wall thickness increases for all three cases (constant l_o, l_i, $(l_o - l_i)/2$), each nanobox exhibits the expected trend with varying VR/TV.

For the constant wall thickness nanoboxes, both the yield stress and yield strain show a decreasing trend with increasing VR/TV. The yield strain again decreases due to an increase in surface area with increasing VR/TV. The modulus for the constant thickness ⟨110⟩ nanoboxes is fairly constant over the range of VR/TV considered in this work, as seen in figure 5(A); thus, the rapid decline in yield strain overrides the slight increase in modulus with VR/TV, leading to the decreasing trend in yield stress as seen in figure 6(A).

As observed in figure 7, the yield strains for the ⟨110⟩ nanoboxes are lower than those of the corresponding solid ⟨110⟩ nanowires; we attribute this to the larger surface area exposed by the nanoboxes. In contrast, the yield stresses of the ⟨110⟩ nanoboxes are generally greater than those of the corresponding solid ⟨110⟩ nanowires. While the yield strains are reduced, the elevated stiffness exhibited by the ⟨110⟩ nanoboxes enables the nanoboxes to sustain larger stresses before initial yield.

4. Conclusions

In conclusion, we have utilized molecular statics calculations in conjunction with an embedded atom potential for copper to characterize the elastic properties of hollow metal nanowires, or nanoboxes. It was illustrated that knowledge of the relative strengths of the bulk material as compared to the surfaces could be utilized to create high strength, lightweight nanostructures by removing the bulk material from the nanowires.

This theory was illustrated through consideration of nanoboxes with two different orientations, ⟨100⟩ and ⟨110⟩. The ⟨100⟩ nanoboxes were found to be elastically softer than the corresponding solid ⟨100⟩ nanowires for all cases. However, the ⟨110⟩ nanoboxes showed modulus increases as compared to the corresponding solid ⟨110⟩ nanowires; the

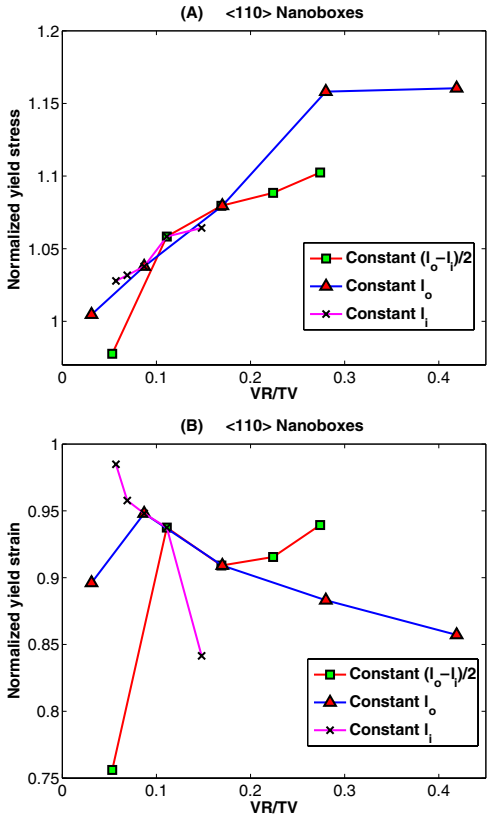

Figure 7. Variation of the (A) normalized yield stress and (B) normalized yield strain for ⟨110⟩ nanoboxes with VR/TV ratio.

largest modulus increases were found to be of the order of 20% for the ⟨110⟩ nanoboxes considered in this work. This behaviour is possible due to the knowledge that, while the ⟨100⟩ bulk is stronger than the {100} surfaces, thus giving no strength advantage to the nanoboxes, the ⟨110⟩ bulk is weaker than the corresponding {110} surfaces. Thus, removal of the ⟨110⟩ bulk leads to the observed strength increases for the ⟨110⟩ nanoboxes.

The nanobox yield stresses were found, for the ⟨110⟩ orientation, to exceed those seen in the corresponding solid ⟨110⟩ nanowires, while the ⟨100⟩ nanobox yield stresses were lower than those of the solid ⟨100⟩ nanowires. In contrast, the nanobox yield strains for both orientations were found to be lower than those of the corresponding solid nanowires. This yield strain reduction is attributed to the larger amount of surface area of the nanoboxes; larger amounts of surface area contribute to a higher probability of defect generation from the surfaces, thus leading to lower yield strains. The enhanced yield stresses of the ⟨110⟩ nanoboxes thus occurs due to the rapid escalation of the nanobox modulus with increasing VR/TV ratio.

We note that, as the experimental synthesis of hollow metal nanostructures is in its infancy, and because it is currently unknown as to the optimal geometries (longitudinal and surface orientations) of hollow nanostructures, the results reported in this work should be regarded at present as qualitative rather than quantitative. Future work will concentrate on determining the inelastic response and controllable mechanical functionality of the various nanoboxes considered; such work will be valuable due to recent results [22, 44] indicating that both geometry and surface orientation can have first-order effects on the inelastic deformation of metal nanostructures.

Acknowledgments

The authors gratefully acknowledge funding from the Vanderbilt University Discovery Grant in support of this research.

References

[1] Canham L T 1990 Silicon quantum wire array fabricated by electrochemical and chemical dissolution of wafers *Appl. Phys. Lett.* **57** 1046–8
[2] Xia Y, Yang P, Sun Y, Wu Y, Mayers B, Gates B, Yin Y, Kim F and Yan H 2003 One-dimensional nanostructures: synthesis, characterization, and applications *Adv. Mater.* **15** 353–89
[3] Lieber C M 2003 Nanoscale science and technology: building a big future from small things *MRS Bull.* **28** 486–91
[4] Li D, Wu Y, Kim P, Shi L, Yang P and Majumdar A 2003 Thermal conductivity of individual silicon nanowires *Appl. Phys. Lett.* **83** 2934–6
[5] Brandbyge M, Schiotz J, Sorensen M R, Stoltze P, Jacobsen K W, Norskov J K, Olesen L, Laegsgaard E, Stensgaard I and Besenbacher F 1995 Quantized conductance in atom-sized wires between two metals *Phys. Rev.* B **52** 8499–514
[6] Wong E W, Sheehan P E and Lieber C M 1997 Nanobeam mechanics: elasticity, strength, and toughness of nanorods and nanotubes *Science* **277** 1971–5
[7] Cuenot S, Frétigny C, Demoustier-Champagne S and Nysten B 2004 Surface tension effect on the mechanical properties of nanomaterials measured by atomic force microscopy *Phys. Rev.* B **69** 165410
[8] Wu B, Heidelberg A and Boland J J 2005 Mechanical properties of ultrahigh-strength gold nanowires *Nat. Mater.* **4** 525–9
[9] Ikeda H, Qi Y, Cagin T, Samwer K, Johnson W L and Goddard W A III 1999 Strain rate induced amorphization in metallic nanowires *Phys. Rev. Lett.* **82** 2900–3
[10] Landman U, Luedtke W D, Burnham N A and Colton R J 1990 Atomistic mechanisms and dynamics of adhesion, nanoindentation, and fracture *Science* **248** 454–61
[11] Branicio P S and Rino J P 2000 Large deformation and amorphization or Ni nanowires under uniaxial strain: a molecular dynamics study *Phys. Rev.* B **62** 16950–5
[12] Kang J-W and Hwang H-J 2001 Mechanical deformation study of copper nanowires using atomistic simulation *Nanotechnology* **12** 295–300
[13] Wu H A, Soh A K, Wang X X and Sun Z H 2004 Strength and fracture of single crystal metal nanowire *Key Eng. Mater.* **261–263** 33–8
[14] Liang W and Zhou M 2004 Response of copper nanowires in dynamic tensile deformation *Proc. Inst. Mech. Eng.* C **218** 599–606
[15] Sanchez-Portal D, Artacho E, Junquera J, Ordejon P, Garcia A and Soler J M 1999 Stiff monatomic gold wires with a spinning zigzag geometry *Phys. Rev. Lett.* **83** 3884–7
[16] da Silva E Z, da Silva A J R and Fazzio A 2001 How do gold nanowires break? *Phys. Rev. Lett.* **87** 256102
[17] Park H S and Zimmerman J A 2005 Modeling inelasticity and failure in gold nanowires *Phys. Rev.* B **72** 054106
[18] Mehrez H and Ciraci S 1997 Yielding and fracture mechanisms of nanowires *Phys. Rev.* B **56** 12632–42
[19] Gall K, Diao J and Dunn M L 2004 The strength of gold nanowires *Nano Lett.* **4** 2431–6

[20] Diao J, Gall K and Dunn M L 2004 Yield asymmetry in metal nanowires *Nano Lett.* **4** 1863–7

[21] Coura P Z, Legoas S G, Moreira A S, Sato F, Rodrigues V, Dantas S O, Ugarte D and Galvao D S 2004 On the structural and stability features of linear atomic suspended chains formed from gold nanowires stretching *Nano Lett.* **4** 1187–91

[22] Park H S, Gall K and Zimmerman J A 2006 Deformation of FCC nanowires by twinning and slip *J. Mech. Phys. Solids* **54** 1862–81

[23] Zhou L G and Huang H 2004 Are surfaces elastically softer or stiffer? *Appl. Phys. Lett.* **84** 1940–2

[24] Liang H, Upmanyu M and Huang H 2005 Size-dependent elasticity of nanowires: nonlinear effects *Phys. Rev.* B **71** 241403(R)

[25] Diao J, Gall K and Dunn M L 2003 Surface-stress-induced phase transformation in metal nanowires *Nat. Mater.* **2** 656–60

[26] Liang W, Zhou M and Ke F 2005 Shape memory effect in Cu nanowires *Nano Lett.* **5** 2039–43

[27] Park H S 2006 Stress-induced martensitic phase transformation in intermetallic nickel aluminum nanowires *Nano Lett.* **6** 958–62

[28] Park H S, Gall K and Zimmerman J A 2005 Shape memory and pseudoelasticity in metal nanowires *Phys. Rev. Lett.* **95** 255504

[29] Koh A S J and Lee H P 2006 Shock-induced localized amorphization in metallic nanorods with strain-rate-dependent characteristics *Nano Lett.* **6** 2260–7

[30] Gai P L and Harmer M A 2002 Surface atomic defect structures and growth of gold nanorods *Nano Lett.* **2** 771–4

[31] Sun Y and Xia Y 2003 Alloying and dealloying processes involved in the preparation of metal nanoshells through a galvanic replacement reaction *Nano Lett.* **3** 1569–72

[32] Sun Y, Mayers B, Herricks T and Xia Y 2003 Polyol synthesis of uniform silver nanowires: a plausible growth mechanism and the supporting evidence *Nano Lett.* **3** 955–60

[33] Gao Y *et al* 2003 Synthesis, characterization and self-assembly of silver nanowires *Chem. Phys. Lett.* **380** 146

[34] Kondo Y and Takayanagi K 1997 Gold nanobridge stabilized by surface structure *Phys. Rev. Lett.* **79** 3455–8

[35] Rodrigues V, Fuhrer T and Ugarte D 2000 Signature of atomic structure in the quantum conductance of gold nanowires *Phys. Rev. Lett.* **85** 4124–7

[36] Tommei G E, Baletto F, Ferrando R, Spadacini R and Danani A 2004 Energetics of fcc and decahedral nanowires of Ag, Cu, Ni, and C_{60}: a quenched molecular dynamics study *Phys. Rev.* B **69** 115426

[37] Caswell K K, Bender C M and Murphy C J 2003 Seedless, surfactantless wet chemical synthesis of silver nanowires *Nano Lett.* **3** 667–9

[38] Chen H, Gao Y, Zhang H, Liu L, Yu H, Tian H, Xie S and Li J 2004 Transmission-electron-microscopy study on fivefold twinned silver nanowires *J. Phys. Chem.* B **108** 12038–43

[39] Lee W, Scholz R, Nielsch K and Gosele U 2005 A template based electrochemical method the synthesis of multisegmented metallic nanotubes *Angew. Chem. Int. Edn* **44** 6050–4

[40] Fan H J, Knez M, Scholz R, Nielsch K, Pippel E, Hesse D, Zacharias M and Gsele U 2006 Monocrystalline spinel nanotube fabrication based on the Kirkendall effect *Nat. Mater.* **5** 627–31

[41] Kelly K L, Coronado E, Zhao L L and Schatz G C 2003 The optical properties of metal nanoparticles: the influence of size, shape, and dielectric environment *J. Phys. Chem.* B **107** 668–77

[42] Wiley B, Sun Y, Mayers B and Xia Y 2005 Shape-controlled synthesis of metal nanostructures: the case of silver *Chem. Eur. J.* **11** 454–63

[43] Mook W M, Jungk J J, Cordill M J, Moody N R, Sun Y, Xia Y and Gerberich W W 2004 Geometry and surface state effects on the mechanical response of Au nanostructures *Z. Metallk.* **95** 416–24

[44] Ji C and Park H S 2006 Geometric effects on the inelastic deformation of metal nanowires *Appl. Phys. Lett.* **89** 181916

[45] Leach A M, McDowell M and Gall K 2007 Deformation of top-down and bottom–up silver nanowires *Adv. Funct. Mater.* **17** 43–53

[46] Daw M S and Baskes M I 1984 Embedded-atom method: derivation and application to impurities, surfaces, and other defects in metals *Phys. Rev.* B **29** 6443–53

[47] Daw M S, Foiles S M and Baskes M I 1993 The embedded-atom method: a review of theory and applications *Mater. Sci. Rep.* **9** 251–310

[48] Mishin Y, Mehl M J, Papaconstantopoulos D A, Voter A F and Kress J D 2001 Structural stability and lattice defects in copper: *ab initio*, tight-binding, and embedded-atom calculations *Phys. Rev.* B **63** 224106

[49] Cammarata R C 1994 Surface and interface stress effects in thin films *Prog. Surf. Sci.* **46** 1–38

[50] Zhou M 2003 A new look at the atomic level virial stress: on continuum-molecular equivalence *Proc. R. Soc.* A **459** 2347–92

[51] Zimmerman J A, Webb E B III, Hoyt J J, Jones R E, Klein P A and Bammann D J 2004 Calculation of stress in atomistic simulation *Modelling and Simulation in Mater. Sci. Eng.* **12** S319–32

[52] Diao J, Gall K and Dunn M L 2004 Atomistic simulation of the structure and elastic properties of gold nanowires *J. Mech. Phys. Solids* **52** 1935–62